

# **Electromagnetic Field Computation for Power Transmission Lines Using Quasi-Static Sub-Gridding FDTD Approach**

K N Ramli<sup>1</sup>, R A Abd-Alhameed<sup>2</sup>, C H See<sup>2</sup>, J M Noras<sup>2</sup>, and P S Excell<sup>3</sup>

<sup>1</sup>*Faculty of Electrical and Electronic Engineering, Universiti Tun Hussein Onn Malaysia,  
Parit Raja 86400, Batu Pahat, Johor, Malaysia*

<sup>2</sup>*Antennas and Applied Electromagnetics Research Group,  
Electronics Communications and Information Systems Engineering,  
University of Bradford, Bradford, West Yorkshire, BD7 1DP, UK*

<sup>3</sup>*Glyndwr University, Wrexham, LL11 2AW, Wales, UK*

*Email: khairun@uthm.edu.my, c.h.see2@bradford.ac.uk, r.a.a.abd@bradford.ac.uk*

**Abstract:** A new approach of modelling the electromagnetic wave propagation and the penetration of small objects, are investigated and analysed. The travelling electromagnetic wave from source is simulated by time-dependent Maxwell's solutions. Subgridding technique is imposed at the point of interest for observing the electromagnetic field in high resolution. The computational burden caused by a large number of time steps has been parried by implementing the state of art of quasi-static approach. The induced electromagnetic fields near a buried pipeline runs parallel to a 400 kV power transmission lines are presented, and discussed.

**Indexing Terms:** *quasi-static, subgridding, induced electromagnetic fields, power transmission lines.*

## 1. INTRODUCTION

The sharing of route by power transmission lines and buried utility pipelines has become quite common nowadays. This prompts the question to the public concern as to the effect of transmission lines has on underground pipelines. In some situations, the latter may be very close in proximity to transmission lines. It is thus necessary to take into account the electromagnetic fields induced above the pipelines [1]. Electromagnetic interference can be generated in the pipelines due to the electromagnetic induction between the underground pipelines and transmission lines when they are close to each other in the vicinity.

This work presents the development of a new approach of modelling the source excitation and the penetration of structures by continuous propagating electromagnetic plane waves. The technique incorporates the solution of time-dependent Maxwell's numerical computations and the initial value problem as the structures are illuminated by the plane waves. The propagation of waves from source excitation is simulated by solving a finite-difference Maxwell's equation in the time domain.

In this work, finite-difference time-domain (FDTD) method has been used due to its easiness and potentiality to treat complex geometry structures in the huge calculation region [2]. This method of solving Maxwell's differential equations was first proposed in two-dimensional problems [3] and then utilized in three-dimensional applications [4]. However, the standard FDTD method is incompetent if the details of the geometry need to be modelled due to a global fine mesh. As a result, the total

number of cells increases dramatically. The time step must be reduced to fulfill the Courant stability condition causing the computational time to increase significantly. The discretisation of time step is crucial for accurate determination of the scheme and has to be small enough to resolve different dielectric or metal structures.

A frequency domain integral equation such as method of moments is well suited for modelling complex of antennas in free space [5]. In other words, its strength is solving PEC structures effectively. Generally, it employs a method of weighted residuals. All such techniques begin by establishing trial functions with one or more adjustable parameters, and the residuals are obtained from the differences between trial and true solutions. The parameters are found using minimisation to give the best fit of the trial function. In contrast, the time domain FDTD technique is best suited for modelling electromagnetic fields inside and outside inhomogeneous media, in particular the ground. The presence of arbitrary inhomogeneous objects inside the computational domain does not seriously impact the number of unknowns to be determined.

Many researchers in the past have been prompted to investigate subgridding technique as an analysis approach in the interaction between source and scatterer [6-11]. In general, this technique is used to condense the lattice at the point of interest locally and does not require any analytical formula to be taken into account, and hence it is appropriate for objects of any shape. The residual of the space is filled with

coarse grids. The fields on the boundary between coarse and fine grids are coupled using spatial and temporal interpolations. The regions of the coarse and fine grids are computed by the FDTD method and are kept in time step. A stable subgridding algorithm can refine the mesh locally and improve the accuracy of the result without increasing the computational efforts significantly. It is hence very useful for FDTD code.

FDTD technique has been applied to the high voltage power transmission line analysis in the published literature. The computation of transient electromagnetic fields due to switching within a typical high-voltage air-insulated substation (AIS) was done by using FDTD method [12]. Dedkova and Kriz [13] proposed a new effective approach to evaluate the distribution of voltage and current along the nonlinear transmission line by using FDTD method. An improved technique was proposed by Tang *et al.* [14] to calculate the transient inductive interference in underground metallic pipelines due to a fault in nearby power lines. The frequency-dependent problem in the analysis of transient interference was solved in phase domain based on FDTD method. Lu and Cui [15] used FDTD method to calculate the wave processes of voltage and current distributed along the three-phase 500 kV busbars and the power lines without load in the substation of multi-conductor transmission lines (MTL). The iterative formulas were presented to determine the boundary conditions at the node of the branches. The work was extended to transmission line network and non-uniform line [16]. Vector fitting method was adopted in FDTD to treat with the frequency dependent parameters [17]. In this case, the corresponding voltage

and current recursion formulations in FDTD technique were presented based on the recursive algorithm for time domain convolution. The comparison of transient analysis method using Bergeron's method, FDTD method and time-domain finite-element (TDFE) was discussed in [18]. Numerical results of MTL simulations based on Laplace transform and FDTD method was presented and compared in [19].

The method mentioned above has two main advantages relative to the other modelling approaches. First, it is simple to implement for complicated dielectric or metal structures due to arbitrary electrical parameters can be assigned to each cell on the grid. Second, the entire computational spaces need not to be discretised with a fine grid as it put unreasonable burden on the computer processing time. The ultimate objective of research in this area is to access the appropriateness of the method in determining the amount of electromagnetic penetrating fields between transmission lines and underground utility pipeline. The three-phase transmission lines are modelled as the AC sources and the pipeline as the dielectric material. In this case, the pipeline is defined as the fine grid and the residual spaces as the coarse grid in the computational spaces. The fields between these two grids are unknown in nature and have to be calculated. Interpolation algorithm is thus required between the grids. The aim of the present work is to develop the general code for solving the electric and magnetic fields within arbitrary metal or dielectric structures, while maintaining a boundary of uncertainty low reflection level in two-dimensional approach.

## 2. SUMMARY OF METHODS

### A. Quasi-static Theorem

FDTD technique is not a practical scheme when low frequency is applied due to lengthy simulation time. The computer burden cannot be solved even for reasonable spatial resolution. For example, the spatial resolution of  $\Delta x = \Delta y = \Delta z = 1$  cm is given at 50 Hz power line frequency. The duration of time step required is given from Courant stability criterion,  $\Delta t = \Delta x/c\sqrt{3} = 1.92$  ns. In order to cover one complete cycle, the number of time steps needed is  $N = 1/(f\Delta t) = 1.0 \times 10^7$ . It needs many years to complete the simulation even when run on fast machine. However, a method known as quasi-static approximation proposed by Moerlose *et al.* [20] solve the difficulties. The formulation takes into account the wavelength which is much greater than the object of study. The primary advantage of quasi-static formulation is thus reducing the long simulation time constraint. There have been some early efforts of using quasi-static idea to study the interaction between living tissues exposed to extremely low frequency (ELF) electric fields in the published literature such as [21-23]. The basis of their research dominantly verifies the effectiveness of quasi-static scheme at very low frequency. FDTD comes into play when researches in [24-27] applied the same knowledge. In this case, the dimension of the object of study is at a fraction of the wavelength. An attempt to gain the scheme of using the same technique but at much higher frequencies of 900 MHz and 1800 MHz has been made by Emili *et al.* in 2003 [28]. The theoretical method discussed by the authors in [21-23] has been realised in the present work to approximate the quasi-static FDTD subgridding. In

general, two conditions must be satisfied before applying the quasi-static formulation:

i. The size of the object is a factor of 10 or more, smaller than the wavelength.

ii.  $|\sigma + j\omega\varepsilon| \gg \omega\varepsilon_0$

where:

$\sigma$  is the conductivity of the object (S/m)

$\varepsilon$  is permittivity of the object (F/m)

$\omega$  is the angular frequency (measured in radians per second, with units  $s^{-1}$ )

$\varepsilon_0$  is the free space permittivity ( $8.85 \times 10^{-12}$  F/m)

From the conditions stated above, the electric field components tangent to the surface of the structure and the internal fields are roughly zero compared to the applied field. The external electric field components can be viewed as orthogonal to the structure. From Maxwell's equation with  $\text{div } D = \rho$ , the boundary condition for the normal electric field components at the surface of the region of interest is given by the expression [22-24]:

$$j\omega\varepsilon_0 \hat{n} \cdot \vec{E}_{air} = (\sigma_{tissue} + j\omega\varepsilon_{tissue}) \hat{n} \cdot \vec{E}_{tissue} \quad (1)$$

The '·' symbol in equation (1) basically refers to vector dot product. From this equation with the two stated conditions satisfied, the scaling relationship can be deduced:

$$\vec{E}_{tissue}(f) = \left( \frac{\omega}{\omega'} \right) \left[ \frac{\sigma'(f') + j\omega'\varepsilon(f')}{\sigma(f) + j\omega\varepsilon(f)} \right] \vec{E}'_{tissue}(f') \quad (2)$$

where:

$\vec{E}_{tissue}(f)$  is the resultant internal electric field (V/m)

$\vec{E}'_{tissue}(f')$  is the scaling internal electric field (V/m)

$f$  is the frequency of interest (Hz)

$f'$  is the scaling frequency (Hz)

$\omega$  is the angular frequency of interest ( $s^{-1}$ )

$\omega'$  is the scaling angular frequency ( $s^{-1}$ )

$\sigma$  is the conductivity of the object (S/m)

$\sigma'$  is the scaling conductivity of the object (S/m)

Assuming that  $\omega\varepsilon(f) \ll \sigma(f)$  and  $\omega'\varepsilon(f') \ll \sigma'(f')$ , then equation (2) can be approximated as [38-40]:

$$\vec{E}_{tissue}(f) \cong \left[ \frac{f\sigma'(f')}{f'\sigma(f)} \right] \vec{E}'_{tissue}(f') \quad (3)$$

It can be concluded that from this equation, a higher working scaling frequency  $f'$  which falls within the quasi-static region can be chosen to excite the model in order to reduce the computational burden. Hence, the scaling internal electric field which is calculated at much higher frequency can be shifted back to the actual power line

frequency.

### *B. Validation of Subgridding Method*

The main grid of the computational domain was basically divided into subgrids, and the missing fields on the boundary between them are predicted using temporal and spatial interpolations. The average electrical characteristics were considered between the main grid cells and fine grid (subgridding cells) when dielectric material (in this case the pipeline) was present on the interface surface. The field components will be updated on both the main grid and subgridding cells as shown in Figure 1.

Subgrid technique was validated by illustrating example in two cases. Case 1 was considered when the observed field was located inside subgrid area with two conditions: (a) Without subgrid, and (b) With subgrid, as shown in Figure 2 (refers to the x symbol inside the grid region). Case 2 was considered when the observed field was located outside subgrid area with two conditions: (a) Without subgrid, and (b) With subgrid, as depicted in Figure 2 (refers to the x symbol outside the grid region). The problem space was excited by sinusoidal wave and gaussian pulse at 1800 MHz. The electric fields at the same point for case 1 and case 2 were observed and compared as illustrated in Figures 3(a). The magnetic fields at the same point for case 1 and case 2 were also observed and compared as illustrated in Figures 3(b).

The electric fields in subgrid region ( $E_{zg}$ ) and at normal grid ( $E_z$ ) for case 1 were

found to be identical to each other to confirm the proof of concept. The electric fields  $E_z$  with and without subgrid for case 2 were also found to be identical to each other. A similar explanation also applies for the magnetic fields for both case 1 and 2. The results in Figure 4 illustrate the stability of the simulation inside the problem space. The electric field remained at 0.23 V/m when using different values of subgrid cells to justify that the results converge with the mesh size in the computational domain.

### 3. RESULTS AND DISCUSSION

A source code was written to implement the design and analysis of the interaction between overhead high voltage power transmission lines and buried utility pipeline. Fortran 90 was used as a programming language platform. The work was devoted to 2-D TM case. Figure 5 illustrates the cross section and the dimension of a common corridor in which a buried utility pipeline runs parallel to a 400 kV overhead power transmission line. It is designed with low height construction. The height from the ground to the bottom conductors is 17 m.

The distance from the overhead ground wire to the earth surface is 32 m. Phase A conductors at the top were collocated horizontally with a separation of 3.0 m. The bottom conductors of phase B, phase B to C and phase C were collocated horizontally with a separation of 1.75 m, 3.5 m and 1.75 m between two adjacent conductors respectively. The three phase steel lattice transmission high voltage suspension tower

was designed with 6 cables. These cables were used as the source signal which propagates inside the problem space. Each of the 2 cables carries the same phase of the AC current. The general equations of phase *A*, phase *B* and phase *C* cables were given respectively by the expressions:

$$\text{Phase } A = \sin(2\pi ft) \quad (4)$$

$$\text{Phase } B = \sin\left(2\pi ft + \frac{2}{3}\pi\right) \quad (5)$$

$$\text{Phase } C = \sin\left(2\pi ft + \frac{4}{3}\pi\right) \quad (6)$$

where  $f$  is the frequency (Hz) and  $t$  is the time (s). The pipeline was separated at a distance of 100 m from the steel lattice suspension towers and buried 2 m beneath the surface of the earth. It was made from metal with a very high conductivity of  $4.75 \times 10^6$  S/m. The radius of the pipeline was 25 cm.

The soil in the common corridor was designed to be inhomogeneous. It was modelled with different relative permittivity by means of random number generator. It was known that the relative permittivity of soil varies from 1 to 5 at 460 kHz, where as the conductivity is kept at  $2.0 \times 10^{-3}$  S/m [31]. Figure 6 represents a histogram that indicates the number of occurrence that soil with their respective value of random

relative permittivity from 1 to 5. Figure 7 depicts the cumulative distribution function of soil relative permittivity. The plot is basically based on equation (7). The representation of Figures 6 and 7 clearly indicates that the soil was designed as arbitrarily inhomogeneous. The cumulative distribution function (CDF) is given by:

$$CDF(x) = \int_1^{x_1} \frac{1}{4} dx \quad (7)$$

where  $x_1$  is the variable of which is unknown in nature and must be determined by using random number generator. Basically, random number generator is given by the expression:

$$R_g(0 \rightarrow 1) = \frac{1}{4}(x_1 - 1) \quad (8)$$

where  $R_g(0 \rightarrow 1)$  is the random number generator that generates random number from zero to one. Rearranging equation (8), the  $x_1$  term can be deduced as:

$$x_1 = 4R_g(0 \rightarrow 1) + 1 \quad (9)$$

In addition, the conductivity of soil mainly depends on the water content in it and slightly on the granularity. In general, its value was very small typically in the order of  $2.0 \times 10^{-3}$  S/m or less [31]. Homogeneous soil also was used in order to compare the correlation between the neighbouring cells. It was modelled with  $\epsilon_r = 3.0$  while its conductivity remained the same value as before. The computational region at the

coarse grids was discretised at a spatial resolution of 2,609 cells per wavelength ( $\Delta y = \Delta z = 25$  cm). Subgridding involves local mesh refinement in the pipeline and some part of the ground in order to determine the propagation of the waves inside that area while observing the change in the electric and magnetic fields. The computational space for main region was 521 cells  $\times$  185 cells (130.25 m  $\times$  46.25 m) as shown in Figure 8. The subgrid computational space was 40 subgrid cells  $\times$  40 subgrid cells as illustrated in Figure 9. In other words, there were many colours that represent random distribution of the soil. In contrast, the non-colour (white area) depicts the pipeline. The values for the other parameters were summarised in Table 1. The distribution of ground surrounding the pipeline was generated by using random number to simulate the inhomogeneity of the media. The fine grids was discretised at a spatial resolution of 10,435 cells per wavelength ( $\Delta y = \Delta z = 6.25$  cm). In other words, the ratio of the coarse to the fine grids was 4:1. The length of the coarse grids remained at  $3.83 \times 10^{-4}$  of the wavelength. The length of the fine grids remained at  $9.58 \times 10^{-5}$  of the wavelength. The induced EM fields section above the pipeline were observed for 30 cells  $\times$  20 cells (7.5 m  $\times$  5 m). The Courant stability condition for 2-D case is given by:

$$\Delta t \leq \frac{h}{c\sqrt{2}} \quad (10)$$

where  $h$  is the spatial homogeneous FDTD grid ( $h = \Delta y = \Delta z$ ) and  $c$  is the speed of light in free space. According to this equation, the time step was set at 0.4 ns to satisfy the Courant stability condition. The simulation was run for 21,160 time steps to allow

for the wave to fully traverse the spatial domain for 4 cycles.

The interaction results between 400 kV steel suspension towers and metallic cylinder are presented in this section. The frequency of 460 kHz was employed to get the fields before they were altered back to 50 Hz. Figure 10 shows the three-phase 400 kV sinusoidal sources separated by  $120^\circ$  phase shift. The fields  $E_{zg}$ ,  $H_{yg}$  and  $H_{xg}$  were observed at point (31.25 cm, 31.25 cm) within subgrid section. These fields distribution were plotted in Figure 11 for homogeneous and random distribution soil. The EM wave which travels from the suspension tower to the pipeline varies from  $2.24 \times 10^{-7}$  V/m (-133 dBV/m) to  $6.3 \times 10^3$  V/m (76 dBV/m). The distribution of the electric field  $E_z$ , magnetic fields  $H_y$  and  $H_x$  through the simulated FDTD computational space were given in Figure 13 (a), (b) and (c) respectively. In subgrid region, the distribution of  $E_{zg}$ ,  $H_{yg}$  and  $H_{xg}$  were demonstrated in Figure 14 (a), (b) and (c) respectively. Here, the fields inside the metallic pipeline were also found to be zero. The reason for this phenomenon was due to the excess electrons at the surface of the metal preventing any incoming propagating waves from penetrating the pipeline.

It was shown that the electric field distribution surrounding the pipeline alters from  $7.9 \times 10^{-7}$  V/m (-122 dBV/m) to  $7.9 \times 10^{-4}$  V/m (-62 dBV/m) which shows good conformity with [32]. The difference in relative distance of each phase from the nearby pipeline can create phase imbalance in the transmission line. Under fault condition, the currents on the faulty phases of transmission lines were high causing induced AC

voltage on the pipeline. The induced field will not contribute to shock hazard in normal condition. Figures 15 (a), (b) and (c) illustrate the induced EM fields for  $E_z$ ,  $H_y$  and  $H_x$  respectively. As can be seen, the current amplitude induced on the pipe varies ( $H_y$  magnetic fields in figure 15(b)) from  $1.8 \times 10^{-8}$  A/m (-155 dBA/m) to  $1.3 \times 10^{-7}$  A/m (-138 dBA/m), and ( $H_x$  magnetic fields in figure 15(c)) from  $5.6 \times 10^{-8}$  A/m (-145 dBA/m) to  $4.0 \times 10^{-7}$  A/m (-128 dBA/m). It is noteworthy that these currents do not produce any sudden risk to a person nearby.

#### 4. CONCLUSION

An approach to model the interaction between overhead transmission lines and underground utility pipeline at powerline frequency has been presented. This uses the FDTD technique for the whole structure of the problem combined with subgridding method at the object of interest particularly at the underground pipeline. By implementing a modified version of Berenger's PML, the reflection on the boundary layers inside the spatial FDTD computational region has been successfully decreased, although it is surrounded by lossy penetrable media. The computational burden due to huge number of time steps in the order of tens of millions has been eased to tens of thousands by employing the method called quasi-static approximation scheme. In addition, the use of inhomogeneous soil in the common corridor permits a nontrivial proximity region of authentic ground properties to be simulated. Profound investigation of the interaction between electromagnetic fields and natural or utility

arrangement with different electrical characteristics at different level of spatial resolution can be assisted by such tools. The combination of frequency scaling SGFDTD approach with arbitrary inhomogeneous dielectric volume, and the modified Berenger's PML paves a way as a good candidate model of EM fields interaction modelling for complex geometries.

## References:

- [1] A. W. Peabody and A. L. Verhiel, "The effects of high-voltage AC transmission lines on buried pipelines," *IEEE Transactions on Industry and General Applications*, vol. IGA-7, 1971.
- [2] A. Taflove and S. C. Hagness, *Computational electrodynamics: The finite-difference time-domain method*, 3rd ed. Boston, MA: Artech House, 2005.
- [3] K. S. Yee, "Numerical solution of initial boundary value problems involving Maxwell's equations in isotropic media," *IEEE Transactions on Antennas and Propagation*, vol. AP-14, pp. 302-307, 1966.
- [4] G. Mur, "Absorbing boundary conditions for the finite-difference approximation of the time-domain electromagnetic-field equations," *IEEE Transactions on Electromagnetic Compatibility*, vol. EMC-23, pp. 377-382, 1981.
- [5] S. N. Makarov, S. D. Kulkarni, A. G. Marut, and L. C. Kempel, "Method of moments solution for a printed patch/slot antenna on a thin finite dielectric substrate using the volume integral equation," *IEEE Transactions on Antennas and Propagation*, vol. 54, pp. 1174-1184, 2006.
- [6] K. Ramli, R.A. Abd-Alhameed, C.H. See, P.S. Excell, and J.M. Noras, "Hybrid Computational Scheme for Antenna-Human Body Interaction," *Progress In Electromagnetics Research (PIER)*, vol. 133, pp.117-136, 2013.
- [7] K. Xiao, D. J. Pommerenke, and J. L. Drewniak, "A three-dimensional FDTD subgridding algorithm with separated temporal and spatial interfaces and related stability analysis," *IEEE Transactions on Antennas and Propagation*, vol. 55, pp. 1981-1990, 2007.
- [8] T. Ohtani, K. Taguchi, and T. Kashiwa, "A subgridding technique for the complex nonstandard FDTD method," *Electronics and Communications in Japan Part 2 - Electronics*, vol. 87, pp. 1-9, 2004.
- [9] K. M. Krishnaiah and C. J. Railton, "A stable subgridding algorithm and its application to eigenvalue problems," *IEEE Transactions on Microwave Theory and Techniques*, vol. 47, pp. 620-628, 1999.
- [10] S. M. Wang, F. L. Teixeira, R. Lee, and J. F. Lee, "Optimization of subgridding schemes for FDTD," *IEEE Microwave and Wireless Components Letters*, vol. 12, pp. 223-225, 2002.
- [11] S. Kapoor, "Sub-cellular technique for finite-difference time-domain method," *IEEE Transactions on Microwave Theory and Techniques*, vol. 45, pp. 673-677, 1997.
- [12] B. U. Musa, W. H. Siew, and M. D. Judd, "Computation of transient electromagnetic fields due to switching in high-voltage substations," *IEEE Transactions on Power Delivery*, vol. 25, pp. 1154-1161, 2010.
- [13] J. Dedkova and T. Kritz, "FDTD analysis of a nonlinear transmission line," *Progress in Electromagnetics Research Symposium, Beijing, China*, pp. 282-285, 2009.
- [14] J. Tang, X. Cui, L. Qi, T. Lu, L. Li, P. Zhu, G. Yang, and W. Zhang, "Analysis of transient inductive interference in underground pipelines due to faults on

- nearby power lines," *COMPEL: The International Journal for Computation and Mathematics in Electrical and Electronic Engineering*, vol. 26, pp. 1346-1363, 2007.
- [15] T. Lu and X. Cui, "Transient analysis of wave processes for multi-conductor transmission lines with branches using FDTD," *IEEE International Symposium on Electromagnetic Compatibility*, vol. 2, pp. 699-703, 2000.
- [16] T. Lu, L. Qi, J. Li, and X. Cui, "Application of multi-conductor transmission lines on the transient analysis in power substation," *Asia-Pacific Conference on Environmental Electromagnetics*, pp. 198-201, 2003.
- [17] T. Lu, L. Qi, L. Guo, X. Cui, and X. Gu, "Research on experiments and the FDTD Method of multi-conductor transmission lines for transient analysis," *International Symposium on Electromagnetic Compatibility*, vol. 2, pp. 708-712, 2004.
- [18] C. Jiao and Y. Sun, "Progress in studies of transients analysis method of multiconductor transmission lines," *Progress in Electromagnetics Research Symposium, Beijing, China*, pp. 249-253, 2009.
- [19] J. Dedkova and L. Brancik, "Laplace transform and FDTD approach applied to MTL simulation," *PIERS Online*, vol. 4, pp. 16-20, 2008.
- [20] J. D. Moerlose, T. W. Dawson, and M. A. Stuchly, "Application of the finite difference time domain algorithm to quasi-static field analysis," *Radio Science*, vol. 32, pp. 329-341, 1997.
- [21] W. T. Kaune and M. F. Gillis, "General properties of the interaction between animals and ELF electric fields," *Bioelectromagnetics*, vol. 2, pp. 1-11, 1981.
- [22] A. W. Guy, S. Davidow, G. Y. Yang, and C. K. Chou, "Determination of electric current distributions in animals and humans exposed to a uniform 60-Hz high-intensity electric field," *Bioelectromagnetics*, vol. 3, pp. 47-71, 1982.
- [23] L. Golestani-Rad, B. Elahi, and J. Rashed-Mohassel, "Investigating the effects of external fields polarization on the coupling of pure magnetic waves in the human body in very low frequencies," *BioMagnetic Research and Technology*, vol. 5, pp. 1-5, 2007.
- [24] O. P. Gandhi and J. Chen, "Numerical dosimetry at power-line frequencies using anatomically based model," *Bioelectromagnetics*, vol. 13, pp. 43-60, 1992.
- [25] M. A. Stuchly and T. W. Dawson, "Human organ and tissue induced currents by 60 Hz electric and magnetic fields," *Proceedings of the 19th Annual International Conference of the IEEE Engineering in Medicine and Biology Society*, vol. 6, pp. 2464-2467, 1997.
- [26] T. W. Dawson, K. Caputa, and M. A. Stuchly, "High-resolution organ dosimetry for human exposure to low-frequency electric fields," *IEEE Transactions on Power Delivery*, vol. 13, pp. 366-373, 1998.
- [27] M. E. Potter, M. Okaniewski, and M. A. Stuchly, "Low frequency finite difference time domain (FDTD) for modeling of induced fields in humans close to line sources," *Journal of Computational Physics*, vol. 162, pp. 82-103, 2000.
- [28] C.H. See, R.A. Abd-Alhameed and P.S. Excell, "Computation of

- Electromagnetic Fields in Assemblages of Biological Cells Using a Modified Finite Difference Time Domain Scheme”, *IEEE Transactions on Microwave Theory and Techniques*, vol.55, no.9, pp.1986-1994, Sept. 2007.
- [29] A. J. Pansini, *Power transmission and distribution*, 2nd ed. Georgia: The Fairmont Press Inc., 2005.
- [30] G. A. Gouly, *Visual amenity aspects of high voltage transmission*. Somerset, England: Research Studies Press Ltd., 1990.
- [31] W. M. Middleton and M. E. V. Valkenburg, *Reference data for engineers: Radio, electronics, computer, and communications*, 9th ed. Boston, 2002.
- [32] G. M. Amer, "Novel technique to calculate the effect of electromagnetic field of H.V.T.L. on the metallic pipelines by using EMTP program," *18th International Conference and Exhibition on Electricity Distribution (CIRED)*, Turin, Italy, pp. 1-5, 2005.

#### **Authors' affiliations:**

Author Ramli is with the Faculty of Electrical and Electronic Engineering, Universiti Tun Hussein Onn Malaysia, Parit Raja 86400, Batu Pahat, Johor, Malaysia. Author Abd-Alhameed, See and Noras are with the Antennas and Applied Electromagnetics Research Group, Electronics Communications and Information Systems Engineering, Bradford University, Bradford, West Yorkshire, BD7 1DP, UK. Author Excell is with Glyndŵr University, Wrexham, LL11 2AW, UK.

**List of Table and Figure captions:**

**TABLE 1:** FDTD simulation parameters.

**Figure 1:** The proposed subgridding model with field components distribution between two different mediums.

**Figure 2:** The observed field was located inside/outside subgrid area: (a) Without subgrid, (b) With subgrid.

**Figure 3:** The observed fields: (a) The electric field inside subgrid and at normal grid, (b) The magnetic field inside subgrid and at normal grid.

**TABLE 2:** The observed fields in numerical values: (a) The electric field inside subgrid and at normal grid, (b) The magnetic field inside subgrid and at normal grid.

**Figure 4:**

**Figure 5:** Electric field distribution for different number of subgrid cells in one main FDTD cell.

**Figure 6:** Outline of standard circuit 400 kV steel lattice transmission high voltage suspension towers with normal span of 300 m (low height construction design, not to scale) [29, 30].

**Figure 7:** Histogram of soil relative permittivity.

**Figure 8:** Cumulative distribution function of soil relative permittivity.

**Figure 9:** The main region in the computational domain for 400 kV steel lattice transmission high voltage suspension towers model.

**Figure 10:** The subgrid region in the computational domain for 400 kV steel lattice transmission high voltage suspension towers model.

**Figure 11:** Three-phase sinusoidal sources driven from 400 kV steel lattice transmission high voltage suspension towers.

**Figure 12:** The amplitude of EM fields plotted against time inside subgrid region: (a) Electric field  $E_{zg}$ , (b) Magnetic field  $H_{yg}$  and  $H_{xg}$ .

**Figure 13:** The EM fields distributions in the main FDTD grid: (a)  $E_z$ , (b)  $H_y$  and (c)  $H_x$  components.

**Figure 14:** The EM fields distributions in the subgrid region: (a)  $E_{zg}$ , (b)  $H_{yg}$  and (c)  $H_{xg}$  components.

**Figure 15:** The induced EM fields at 1.75 m above metallic pipeline: (a)  $E_z$ , (b)  $H_y$  and (c)  $H_x$  components.

**TABLE 1:**

Parameter	Measurement
Source frequency	460 kHz
Coarse grids	25 cm
Fine grids	6.25 cm
Refinement factor	4
Time step	0.4 ns
Number of time steps	21,160
Number of cycles	4
Subgrid spatial resolution	40 subgrid cells × 40 subgrid cells
Induced EM fields spatial resolution	30 cells × 20 cells

**Figure 1:**

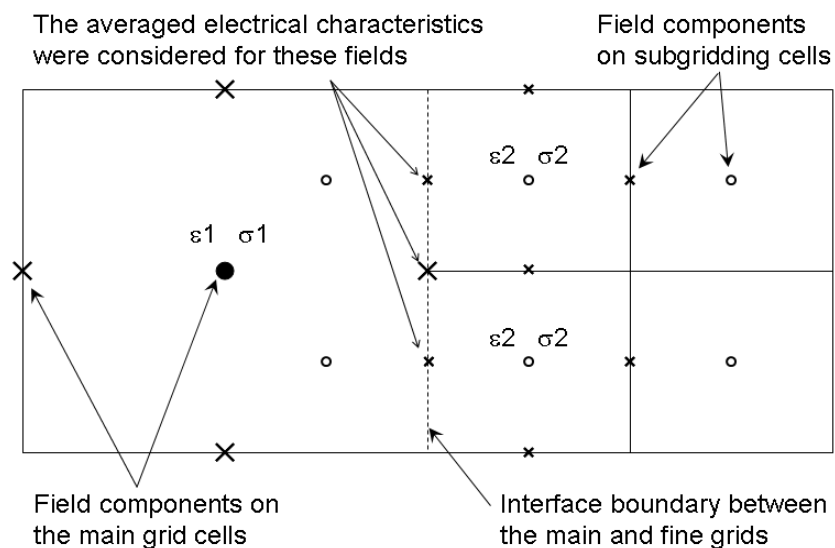
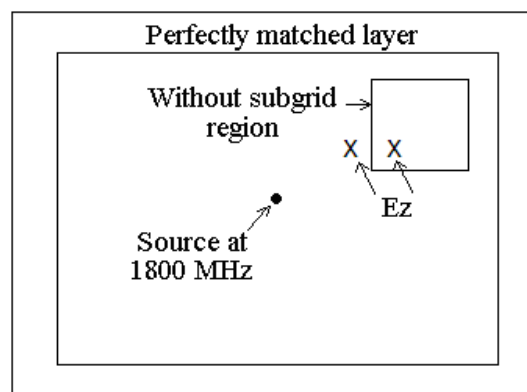
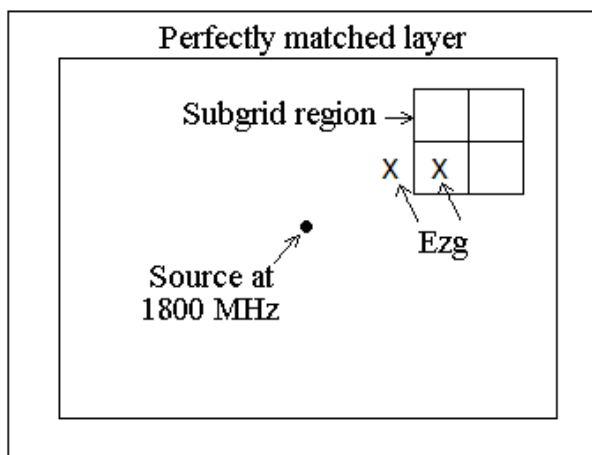


**Figure 2:**

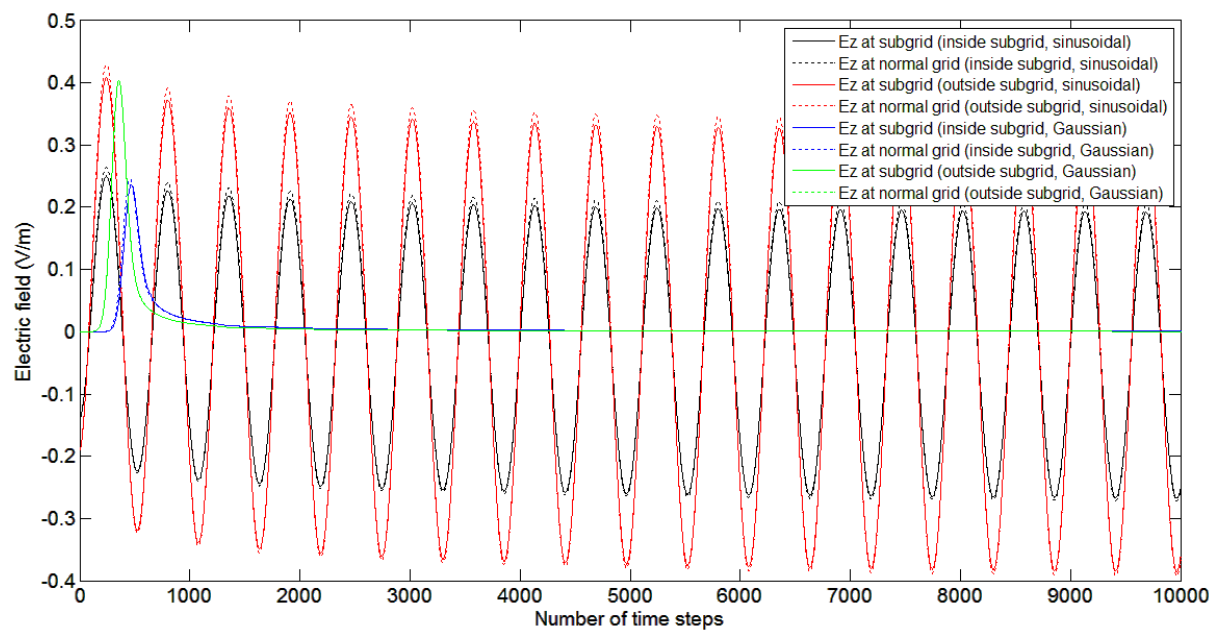


(a)

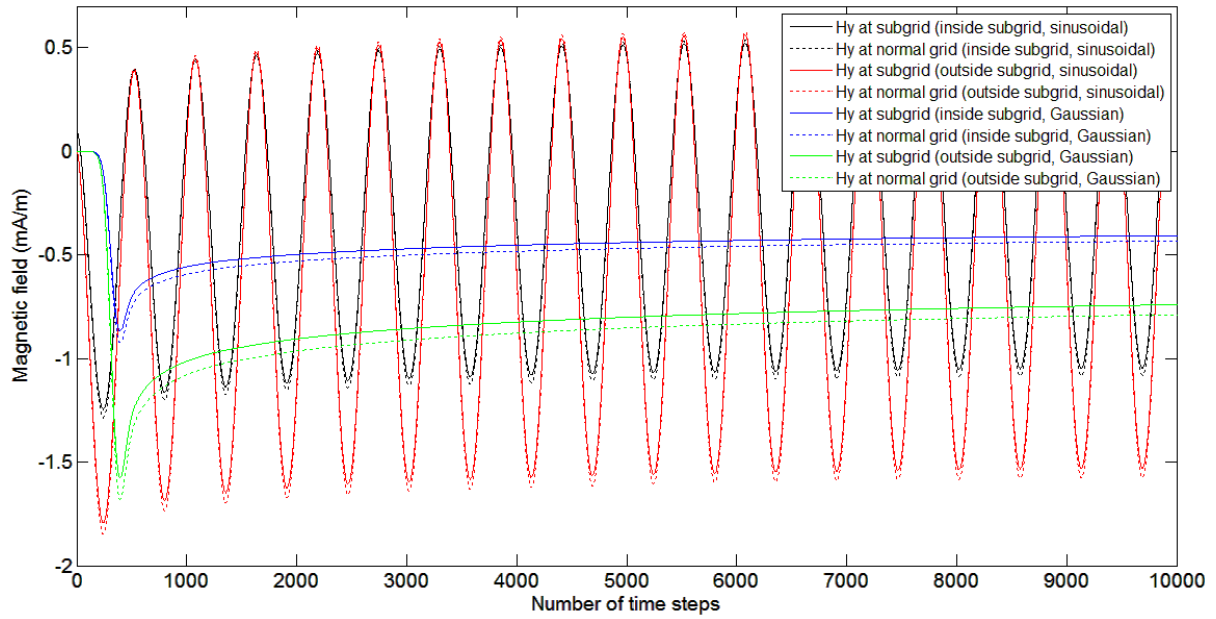


(b)

Figure 3:



(a)



(b)

TABLE 2:

Number of Time Steps	Sinusoidal				Gaussian			
	Inside Subgrid		Outside Subgrid		Inside Subgrid		Outside Subgrid	
	Ez at Subgrid	Ez at Normal Grid	Ez at Subgrid	Ez at Normal Grid	Ez at Subgrid	Ez at Normal Grid	Ez at Subgrid	Ez at Normal Grid
1	-0.1400	-0.1400	-0.1900	-0.1900	-0.1900	0.0087	-0.1900	0.0087
1000	-0.1523	-0.1527	-0.2088	-0.2095	-0.2088	0.0191	-0.2088	0.0135
2000	0.1067	0.1154	0.1881	0.2014	0.1881	0.0061	0.1881	0.0043
3000	0.1994	0.2113	0.3301	0.3483	0.3301	0.0035	0.3301	0.0025
4000	-0.0135	-0.0091	0.0038	0.0106	0.0038	0.0025	0.0038	0.0018
5000	-0.2440	-0.2477	-0.3494	-0.3550	-0.3494	0.0019	-0.3494	0.0013
6000	-0.1781	-0.1794	-0.2483	-0.2504	-0.2483	0.0014	-0.2483	0.0010
7000	0.0899	0.0980	0.1624	0.1747	0.1624	0.0012	0.1624	0.0008
8000	0.1869	0.1983	0.3110	0.3285	0.3110	0.0010	0.3110	0.0007
9000	-0.0233	-0.0192	-0.0111	-0.0049	-0.0111	0.0008	-0.0111	0.0006
10000	-0.2520	-0.2559	-0.3616	-0.3676	-0.3616	0.0007	-0.3616	0.0005

(a)

Number of Time Steps	Sinusoidal		Gaussian	
	Inside Subgrid	Outside Subgrid	Inside Subgrid	Outside Subgrid

	Hy at Subgrid	Hy at Normal Grid	Hy at Subgrid	Hy at Normal Grid	Hy at Subgrid	Hy at Normal Grid	Hy at Subgrid	Hy at Normal Grid
1	0.1000	0.1000	0.0067	0.0067	0.0039	0.0039	0.0055	0.0055
1000	0.1428	0.1441	0.0571	0.0588	0.0571	0.0588	0.0571	0.0588
2000	-0.7502	-0.7757	-1.1335	-1.1675	-1.1335	-1.1675	-1.1335	-1.1675
3000	-1.0701	-1.1052	-1.5602	-1.6070	-1.5602	-1.6070	-1.5602	-1.6070
4000	-0.3365	-0.3496	-0.5820	-0.5995	-0.5820	-0.5995	-0.5820	-0.5995
5000	0.4586	0.4693	0.4781	0.4925	0.4781	0.4925	0.4781	0.4925
6000	0.2316	0.2356	0.1755	0.1808	0.1755	0.1808	0.1755	0.1808
7000	-0.6922	-0.7160	-1.0563	-1.0879	-1.0563	-1.0879	-1.0563	-1.0879
8000	-1.0271	-1.0609	-1.5028	-1.5479	-1.5028	-1.5479	-1.5028	-1.5479
9000	-0.3028	-0.3149	-0.5371	-0.5532	-0.5371	-0.5532	-0.5371	-0.5532
10000	0.4859	0.4975	0.5145	0.5300	0.5145	0.5300	0.5145	0.5300

(b)

Figure 4:

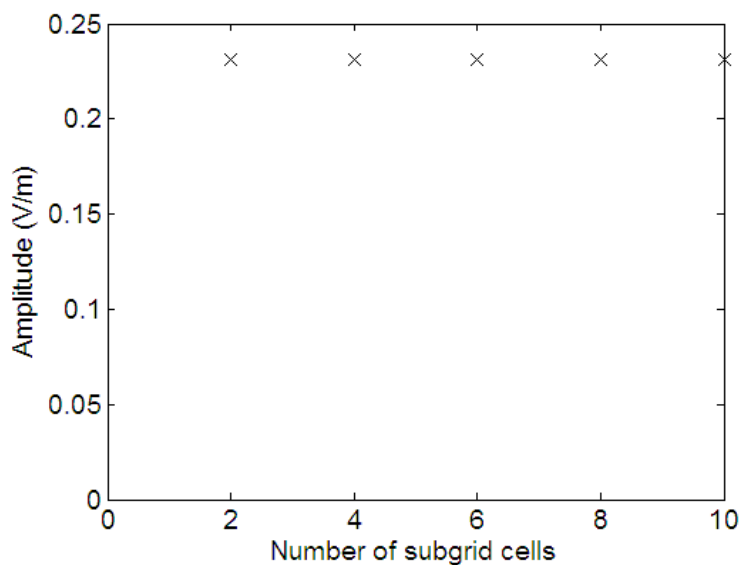


Figure 5:

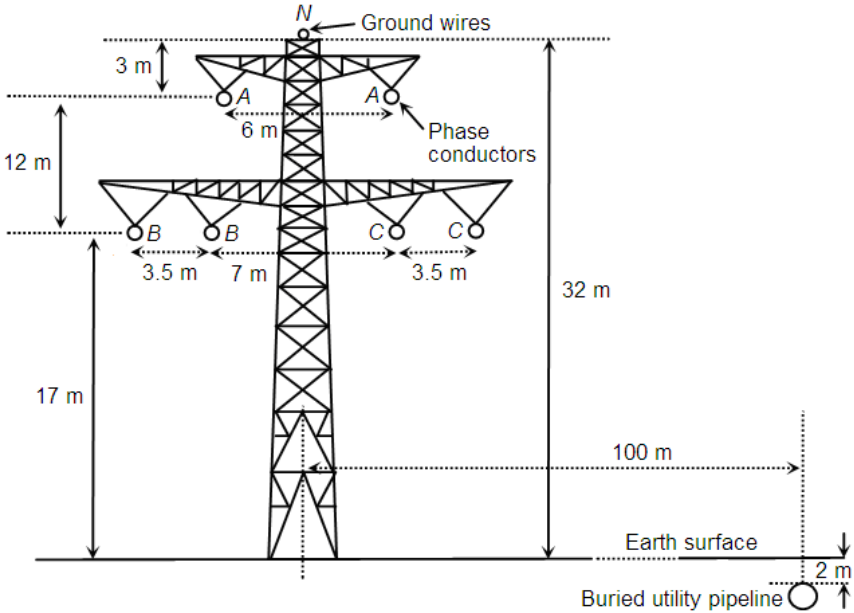
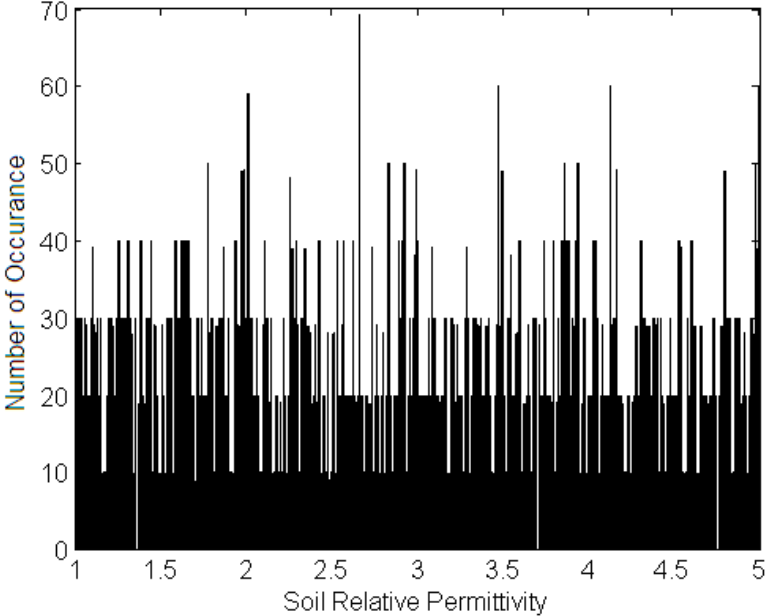
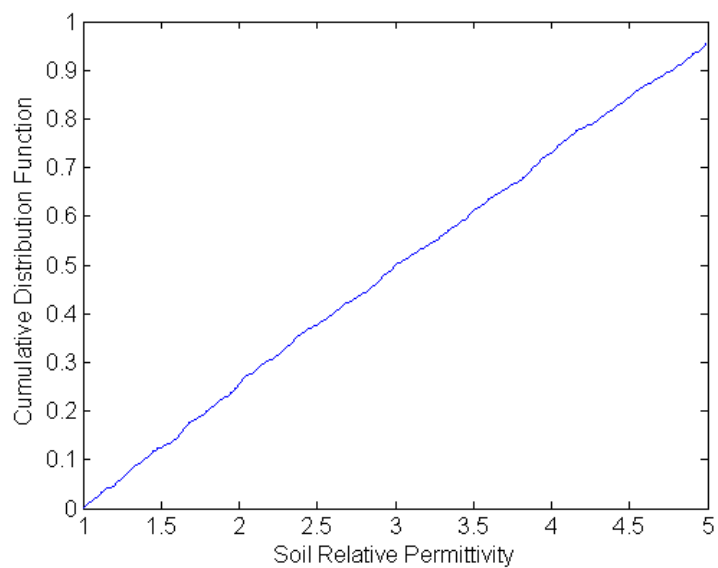


Figure 6:



**Figure 7:**



**Figure 8:**

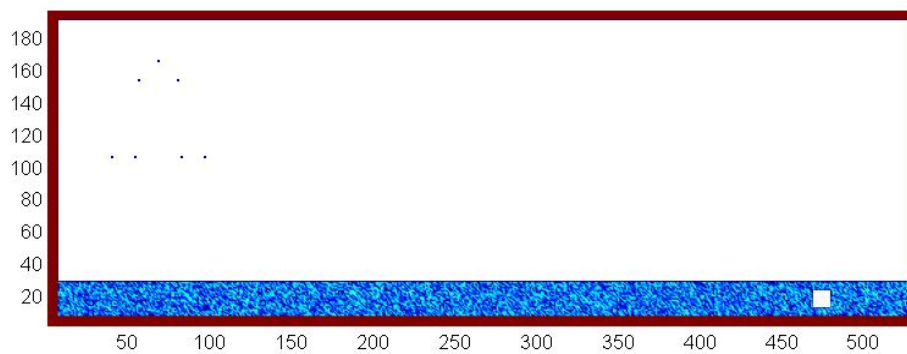


**Figure 9:**

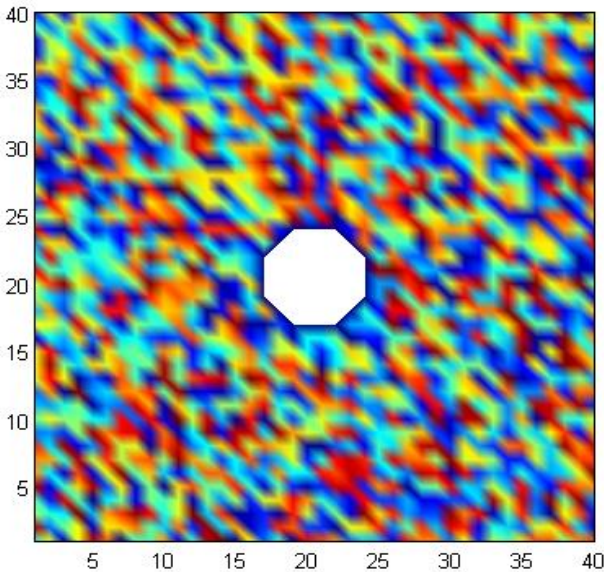


Figure 10:

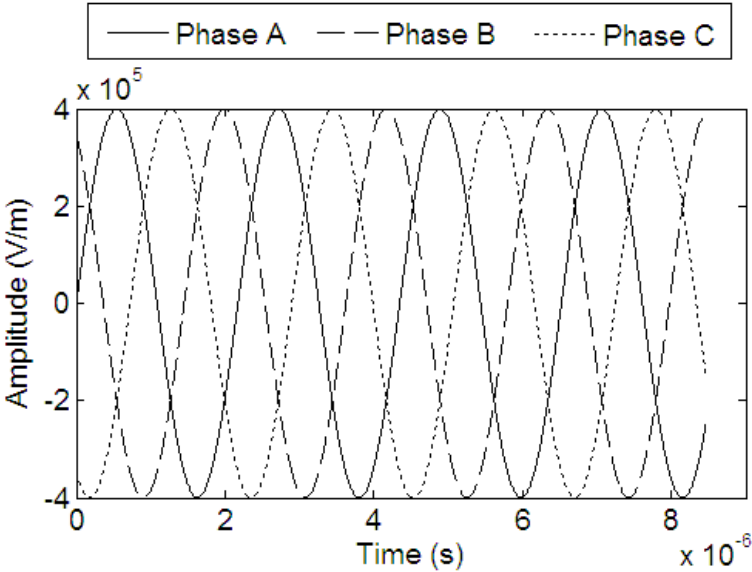
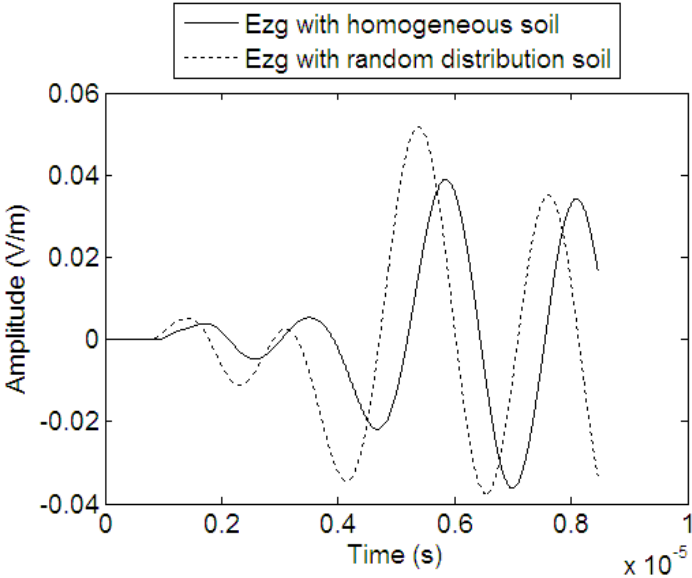
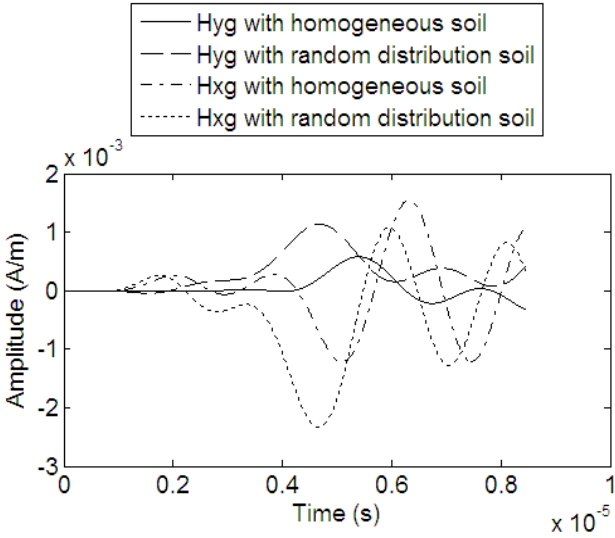


Figure 11:



(a)



(b)

Figure 13:

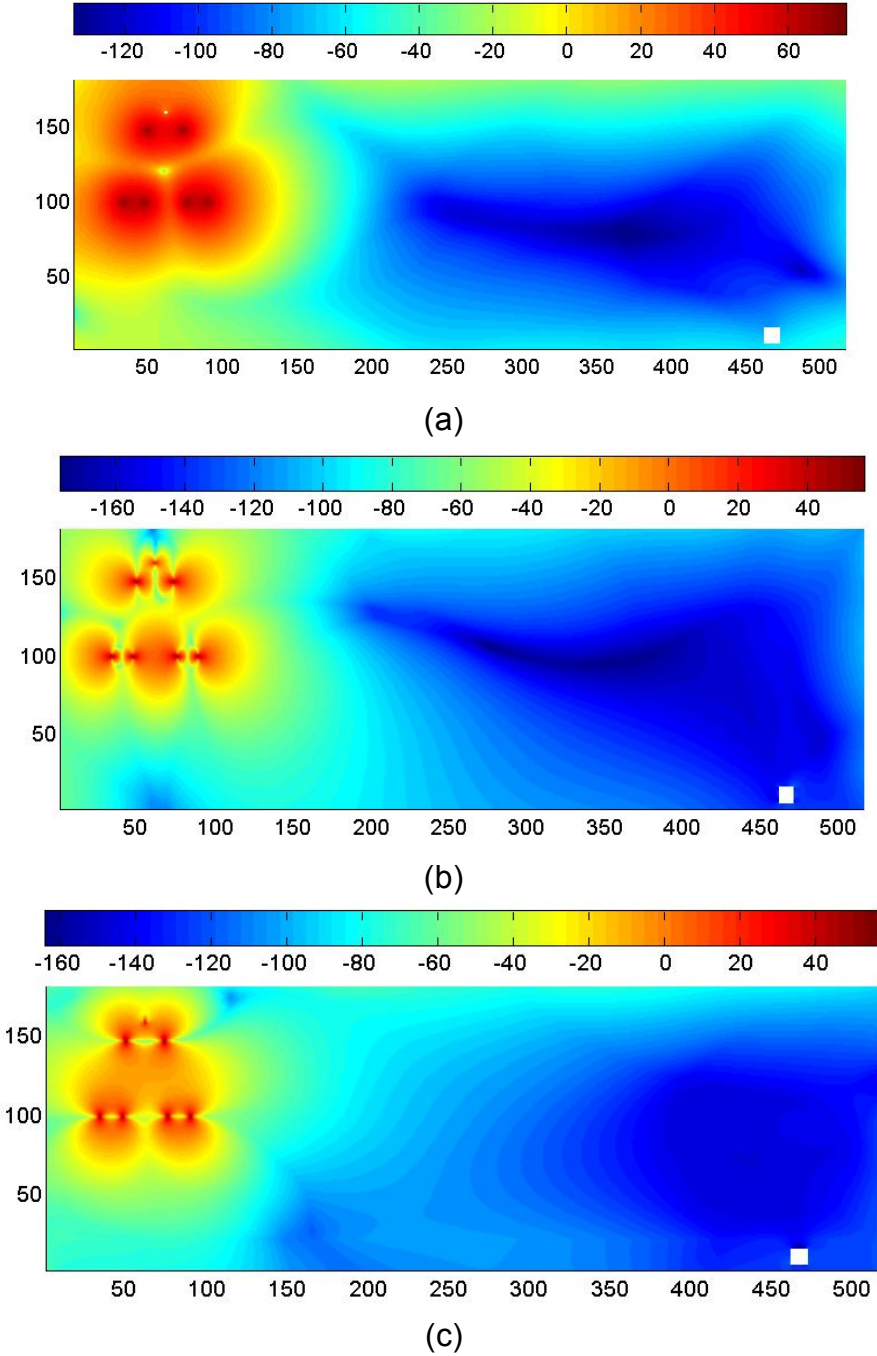
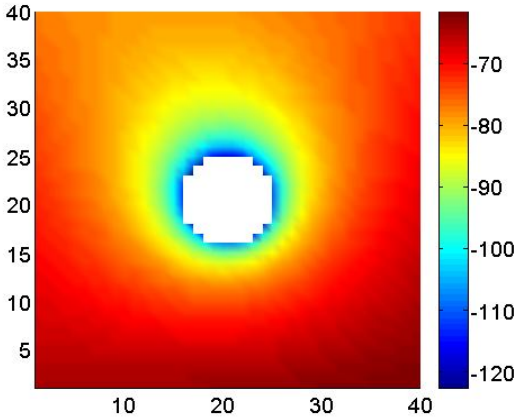
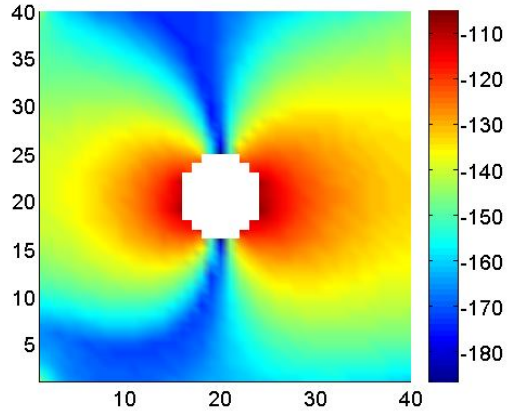


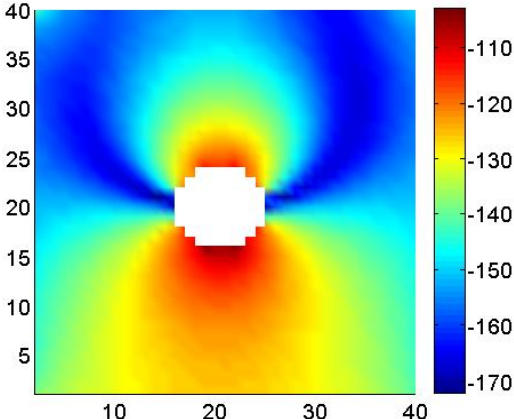
Figure 14:



(a)

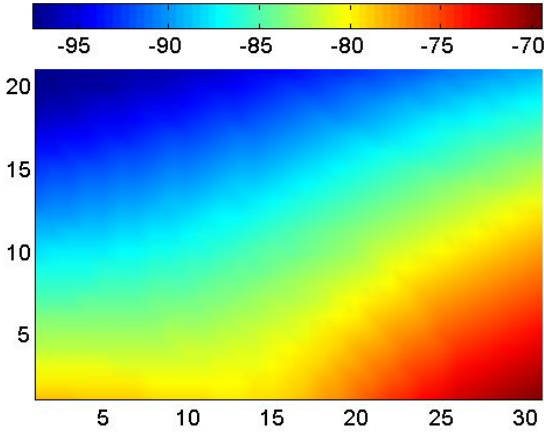


(b)

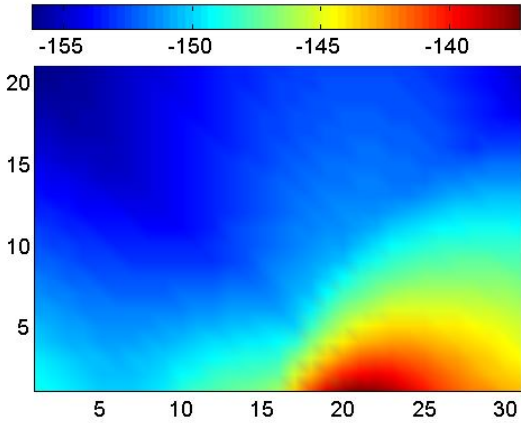


(c)

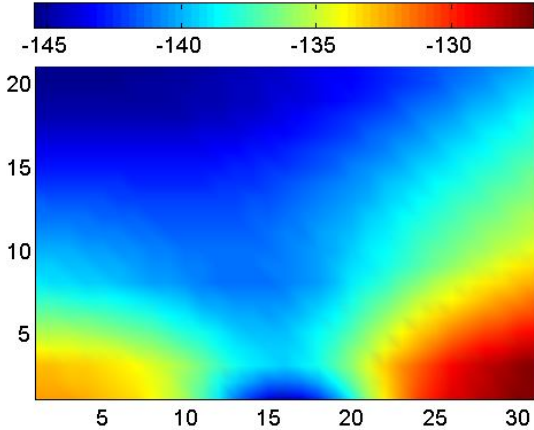
Figure 15:



(a)



(b)



(c)